



Sporadic Spin-orbit Variations in Compact Multiplanet Systems and Their Influence on Exoplanet Climate

Howard Chen^{1,2,3} , Gongjie Li⁴ , Adiv Paradise⁵ , and Ravi K. Kopparapu^{1,2} ¹ Planetary Environments Laboratory, NASA Goddard Space Flight Center, Greenbelt, MD 20771, USA; hchen@fit.edu² GSFC Sellers Exoplanet Environments Collaboration, NASA Goddard Space Flight Center, USA³ Department of Aerospace, Physics, and Space Sciences, Florida Institute of Technology, Melbourne, FL 32901, USA⁴ School of Physics, Georgia Institute of Technology, Atlanta, GA 30332, USA⁵ Department of Astronomy and Astrophysics, University of Toronto, Ontario, Canada

Received 2022 October 20; revised 2023 February 15; accepted 2023 February 16; published 2023 March 29

Abstract

Climate modeling has shown that tidally influenced terrestrial exoplanets, particularly those orbiting M-dwarfs, have unique atmospheric dynamics and surface conditions that may enhance their likelihood to host viable habitats. However, sporadic libration and rotation induced by planetary interactions, such as those due to mean motion resonances (MMR) in compact planetary systems, may destabilize attendant exoplanets away from synchronized states (1:1 spin-orbit ratios). Here, we use a three-dimensional N-rigid-body integrator and an intermediately complex general circulation model to simulate the evolving climates of TRAPPIST-1 e and f with different orbital- and spin-evolution pathways. Planet f scenarios perturbed by MMR effects with chaotic spin variations are colder and dryer compared to their synchronized counterparts due to the zonal drift of the substellar point away from open ocean basins of their initial eyeball states. On the other hand, the differences between perturbed and synchronized planet e are minor due to higher instellation, warmer surfaces, and reduced climate hysteresis. This is the first study to incorporate the time-dependent outcomes of direct gravitational N-rigid-body simulations into 3D climate modeling of extrasolar planets, and our results show that planets at the outer edge of the habitable zones in compact multiplanet systems are vulnerable to rapid global glaciations. In the absence of external mechanisms such as orbital forcing or tidal heating, these planets could be trapped in permanent snowball states.

Unified Astronomy Thesaurus concepts: [Exoplanet atmospheres \(487\)](#); [Planetary climates \(2184\)](#); [Extrasolar rocky planets \(511\)](#); [N-body simulations \(1083\)](#); [Habitable planets \(695\)](#); [Planetary dynamics \(2173\)](#)

Supporting material: animations

1. Introduction

A variety of future observatories are poised to definitively reveal the environmental characteristics of small rocky worlds (Kane 2021). Gas-phase species such as H₂O and CO₂ have already been detected on potentially water-rich and gaseous exoplanets (Kreidberg et al. 2014; Benneke et al. 2019; Edwards et al. 2021; Swain et al. 2021; Fu et al. 2022). For truly terrestrial worlds such as TRAPPIST-1 e and f, simulated detections suggest spectral features of CO₂, CH₄, and N₂O features at the 4.3, 3.3, and 8.5 μm bands will be feasible within 30 transits for near-term observations by the JWST (e.g., Fauchez et al. 2019; Lustig-Yaeger et al. 2019; Wunderlich et al. 2020; Kaltenegger & Lin 2021; Lustig-Yaeger et al. 2022; Mikal-Evans 2022). In the next few years, more potentially habitable planets will be discovered, with the catalog of these systems to date in the order of hundreds and growing; models of various complexities and heritages are just on the rise and will quantitatively evaluate their inhabitation or habitability (Méndez et al. 2020; Fauchez et al. 2021; Wordsworth & Kreidberg 2022; Cooke et al. 2023).

Because of the small orbital separation (semimajor axes) of worlds around M-dwarfs, theory suggests that they will be locked in a synchronized state due to strong tidal forces from the host star. As such, the majority of previous work using

three-dimensional (3D) general circulation model (GCM) to simulate M-dwarf planets assumed 1:1 spin-orbit rotation ratios for planets with short ($\lesssim 50$ days) orbital periods (e.g., Way et al. 2016; Kopparapu et al. 2017; Chen et al. 2019; Yang et al. 2019; Guzewich et al. 2020; Joshi et al. 2020; Cohen et al. 2022; Hammond & Lewis 2021; Lefèvre et al. 2021; Braam et al. 2022; Sergeev et al. 2022; Wolf et al. 2022). This assumption is acceptable due to the computational expense and time-consuming nature of many state-of-the-science GCMs. Slowly and synchronously rotating exoplanets are fascinating model environments for studying unique dynamical features and climate regimes, but there are many means by which their orbits would depart from completely synchronized states. For instance, orbital scattering, merging events, thermal tides, and secular perturbations could drive planets into higher-order spin-orbit resonances (SORs) including 6:1, 2:1, and 3:2 (Leconte et al. 2015; Renaud et al. 2021). Using the 3D climate model Laboratoire de Météorologie Dynamique (LMD), previous publications have found that the stability of tidally influenced exoplanets increases with asynchronous rotation assumptions (e.g., 3:2 spin-orbit ratio; Turbet et al. 2018). Del Genio et al. (2019) however, used the Resolving Orbital and Climate Keys of Earth and Extraterrestrial Environments with Dynamic (ROCKE-3D) model and found that the same resonance case led the lowest global liquid water fractions among all their simulations. Yang et al. (2013) showed, using the National Center for Atmospheric Research climate model Community Climate System Model, that the more rapid rotation rates of 6:1 and 2:1 planets allow the breakup of the



Original content from this work may be used under the terms of the [Creative Commons Attribution 4.0 licence](#). Any further distribution of this work must maintain attribution to the author(s) and the title of the work, journal citation and DOI.

dayside stationary cloud decks, which then destabilizes the energy balance and pushes the planets into runaway states close to the inner edge of the habitable zone (IHZ). Another study, Colose et al. (2021), found that in the absence of internal heating, the IHZ limit is only weakly sensitive to the planet’s spin-orbit resonant state. For tidally heated planets, however, their results show vastly different evolved climates depending on their assumed resonant state.

The orbital evolution of the Sun–Earth system has an intimate relationship with the observed paleoclimate record, also known as Milankovich cycles. From ice core samples (Kawamura et al. 2007), N-body simulations (Laskar et al. 2004), Mars’s polar ice caps (e.g., Toon et al. 1980), and climate modeling (e.g., Spiegel et al. 2010; Deitrick et al. 2018b, 2018a), for example, it has been found that the orbital changes on the 10–10,000 yr timescale have been crucial in understanding the variability in Earth’s climate throughout history.

Along a similar vein, the net orbital motions of distant exoplanets, their host stars, and neighboring rocky bodies exert strong forcings onto their transient and mean climates.⁶ Planetary rotation, for instance, governs cloud distribution, mean cloud cover, and exoplanetary albedo (Yang et al. 2013; Way et al. 2016; Jansen et al. 2019; He et al. 2022) and can strongly affect boundaries of the inner edges of the habitable zone (Yang et al. 2014). Others have found that Earthlike exoplanets can maintain clement temperature at large obliquities (Kilic et al. 2017; He et al. 2022), avoid global glaciation at lower stellar fluxes due to tidal heating (Colose et al. 2019), and even bolster the oxygenation of exo-ecospheres (Barnett & Olson 2022). Varying eccentricity may also have potentially observable climatic effects (Way & Georgakarakos 2017), and large eccentricity combined with obliquity could instigate ice-sheet melting during colder seasons (Shields et al. 2016) and promote marine biological activity (Jernigan et al. 2023). Vervoort et al. (2022) showed how the presence of giant-planet-induced precession cycles can influence the fractional habitability of planets with Earth-similar atmospheres. Using an energy balance model, (Quarles et al. 2022) found that large obliquity variations (i.e., $>55^\circ$) can lead to dynamical transitions to snowball stages due to the large thermal inertia of the ice belt.

Future detection and observational measurements will be biased toward short-period planets. As such, compact systems (e.g., multiple planets with $P < 50$ days) of planets close to the host star serve as blueprints for understanding the diversity of exoplanet system architectures (Kane et al. 2013; Tamayo et al. 2020). Owing to the proximity of planets in these systems, mutual gravitational interactions between neighboring planets can cause spin-axis dynamics that may be crucial from observational and habitability standpoints. For instance, spin-orbit-coupling induced orbital precession can lead to detectable transit-timing variations (Bolmont et al. 2020; Chen et al. 2021b) and compete against tidal forces from the host star (Vinson et al. 2019). To our knowledge, none have previously examined the climate impacts of chaotic spin variations due to planet–planet interactions, especially when they dominate over stellar influences. How might these effects modulate a planet’s rotational state, amplitude and period of orbit, obliquity cycles, atmospheric evolution, ocean circulation, and surface climate?

⁶ Tidal modulations may be important for other reasons, for instance, by influencing the stability of planetary orbits (Lingam et al. 2022).

In this Letter, we use an N-rigid-body integrator and a 3D GCM with reduced complexity to evaluate time-evolving climates of TRAPPIST-1 planets. In Section 2, we describe the numerical models and assumptions. In Section 3, we present the results of our N-rigid-body simulation package and 3D climate model. In Section 4, we discuss the caveats, implications, and observational relevance of this study. We conclude the study in Section 5.

2. Numerical Model, Data, and Methodology

An N-rigid-body integrator with self-gravitating particles is used to model the effects of spin-orbit coupling. Informed by the outcomes derived from these results, a climate model of intermediate complexity is employed to simulate the planetary climates of TRAPPIST-1 e and f.

2.1. GRIT: An N-Rigid-Body Model to Simulate the Spin–Orbit Coupling of Planetary Systems

We use an N-rigid-body simulation package, the Gravitationally interacting Rigid-body InTegrator (GRIT; Chen et al. 2021b), to compute the spin and orbital evolution of TRAPPIST-1 e and f. To account for spin-orbital dynamics and their mutual interactions, GRIT utilizes a Lie–Poisson algorithm starting with first-principal rigid-body dynamics. This integrator is an improvement upon previous seminal work (Touma & Wisdom 1994) by way of relaxing the assumption of strictly near-Keplerian orbits, including any number of objects as rigid bodies in the system, as well as the inclusion of high-order implementations. Refer to Chen et al. (2021b) for the detailed model breakdown.

GRIT is employed to generate the parameters relevant to the planet’s orbital and spin evolution; these parameters include orbital elements (e.g., semimajor axis, eccentricity, and inclination) and spin parameters (e.g., spin rate, spin along the x - y - z -axes, obliquity, and the misalignment of the planetary tidally elongated or long axis). The illustration of the misalignment of the long axis is shown in Figure 1, where a tidally locked planet will have near-zero misalignment. z -axis spin values are directly read as the planetary rotation rate, and the axis misalignment ψ values are translated to the longitude of incident stellar heating (ϕ) via $\phi = 180 + \psi$. The sign of ϕ is calculated using a 3D rotational matrix centered on the z -axis.

We perform three sets of GRIT simulations: TRAPPIST-1e with no tidal dissipation, TRAPPIST-1f with no tidal dissipation, and TRAPPIST-1f with tidal dissipation. Each of these is run for at least 5000 yr, and their solutions are recorded annually. We adopted a constant time-lag model following Eggleton et al. (1998), setting the time lag to be 2×10^{-5} yr (or 638 s, similar to the case of the Earth). We set the Eggleton’s Q number (Q_E) to be 0.23, corresponding to a love number of 0.3 (also similar to that of the Earth).

2.2. ExoPlaSim: A User-friendly and Versatile GCM for Exoplanet Environments

The Exo-Planet Simulator (hereafter ExoPlaSim) is an intermediately complex GCM maintained and developed by Paradise et al. (2022). ExoPlaSim has been modified and adapted for exoplanet environments and characteristics after the original Planet Simulator (PlaSim; Fraedrich et al. 2005).

As GCMs such as ExoPlaSim simulate Earth-system components (i.e., the atmosphere, land, ocean, and sea-ice),

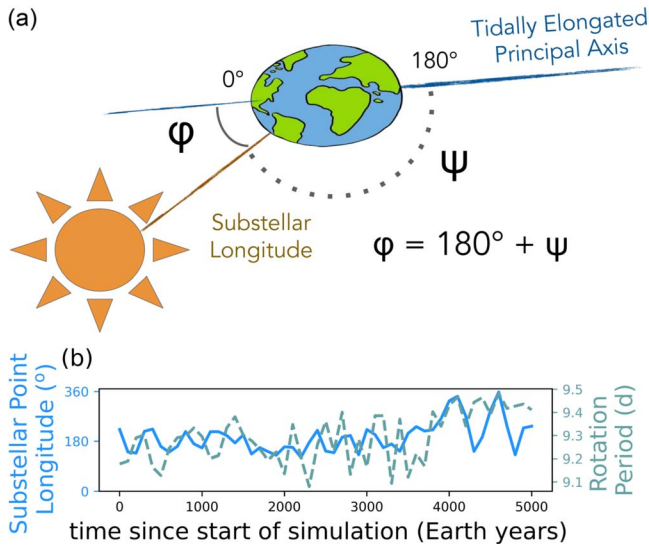


Figure 1. Cartoon schematic illustrating the relationship between ψ , the long-axis misalignment and ϕ , the substellar longitude (a), and example time-series plot showing the variability of substellar longitude and planetary rotation period due to spin-axis dynamics calculated by an N-rigid-body integrator on a 100 yr time step (b). This study explores the effects of variations in ψ and ϕ on exoplanet climate using an intermediately complex Earth system model.

they are advantageous over single-column or one-dimensional climate models. However, simplifications regarding certain parameterizations and processes such as radiative transfer or surface hydrology are made (Poulsen et al. 2001; Vallis et al. 2018; Paradise et al. 2019; Galuzzo et al. 2021). Relaxing these assumptions with an intermediate-complexity GCM is appropriate as our study is not designed to reproduce climate behaviors with high realism nor predict specific exo-atmospheric compositions but rather provide a more generally meaningful result. In addition, such GCMs with reduced complexity permit simulation of key 3D processes including cloud formation, large-scale circulation, moist processes, and climate feedback at a lower computational cost (see, e.g., Biasiotti et al. 2022 for another category of computationally inexpensive but accurate climate models). This will become crucial when we need to compute a diverse range of anticipated exoplanet compositions.

Here, ExoPlaSim is used to simulate Earthlike, CO_2 -dominated, and steam atmospheres⁷ with planet properties (i.e., mass, radius, orbital period) consistent with TRAPPIST-1 e and f (Agol et al. 2021). Orbital eccentricity and precession are set to zero for all planets. For tidally locked planets, we set the rotation periods to be equal to their orbital periods and the substellar point fixed at 180° longitude. For the perturbed planets, we update the rotation period and the substellar point of the planet every 1 Earth yr, with spin values derived from GRIT outputs.

Throughout the paper, we use the original 1:1 unperturbed substellar point (180°) as the reference point for “current” location of the perturbed substellar point. The current substellar point longitude for any perturbed system is equivalent to 180° added or subtracted by the degree of long-axis misalignment

⁷ Even though volatile accretion models suggest a diverse range of atmospheric compositions (Chen & Jacobson 2022), our goal is not to make any definitive predictions on them. Rather, these compositions are set to allow clement surface temperatures to arise (while avoiding the moist greenhouse threshold) to facilitate comparison between modeling results.

(ϕ) with the direction toward the star. The “dayside hemisphere” refers to between $+90^\circ$ and $+270^\circ$ longitude, regardless of the actual location of stellar insolation.

For planet e, we simulate three scenarios with Earthlike atmospheric compositions: aquaplanet (control), desert planet (i.e., 100% land cover), and an aquaplanet with 1:1 synchronized orbits. For planet f, we simulate 33 bar CO_2 (control) and a 33 bar CO_2 plus 1 bar H_2O composition.⁸ The aquaplanets use a 30 m thermodynamic slab ocean model, and desert planets have constant surface albedo values of 0.2 (Paradise et al. 2022). The majority of the results will be focused on comparing the control runs with one or two of the sensitivity experiments. We also test the effects of two different stellar spectral energy distributions (SEDs).

For the Sunlike star SED, we use a reconstructed solar irradiance spectrum from Lean et al. (1995). The input spectrum version is fixed in the year 1850, and no observed irradiance cycle is included. For the SED of the TRAPPIST-1-like star, we downloaded pregenerated spectra from the BT-Settl database. This spectra has stellar metallicity of $[\text{F}/\text{H}] = 0.0$, alpha enhancement of $[\alpha/\text{M}] = 0.0$, surface gravity $\log g = 4.0$, and stellar effective temperature (T_{eff}) of 2600 K.

All ExoPlaSim simulations use an exponential filter, which is applied both at the transform from grid-point space to spectral space and then from spectral space back to grid-point space. Appendix A of Paradise et al. (2022) states that at T21 and T42 resolutions, exponential and Lander–Hoskins filters have very similar performance, with the former working better for slower rotators (>7 days). We set the T21 horizontal resolutions with vertical domains extending up to 0.01 bar. All simulations (including those shown and not shown) are integrated for at minimum 300 Earth yr and maximum of 800 Earth yr (hereafter, years will refer to Earth years). We consider the radiative balance to be at equilibrium after the 30 yr mark.

2.3. Leveraging N-Rigid-Body Outputs in the 3D Climate Model: Some Details and Caveats

The climate model was used to simulate a 400 yr time slice from the full 5000 yr GRIT output. TRAPPIST-1 e control and TRAPPIST-1 f used 4600–5000 yr to examine the later stages of orbital evolution when the systems have been sufficiently excited. The “younger” planet f used the same GRIT output as the control but started at time zero; the simulation with high tidal dissipation also started at time zero. Changes to substellar forcing informed by GRIT results are applied as soon as each climate model run starts, and these changes are updated every year according to these solutions.

Effects due to eccentricity variations and precession, while not explicitly calculated, are reflected in our spin-misalignment calculation. Specifically, ψ is the long-axis misalignment with respect to the direction toward the star, and the direction toward the star is calculated based on the orbital location of the planet, which is affected by eccentricity and orbital precession. We do not include obliquity variations in this study since the planets do not acquire large obliquities (the maximum obliquity of TRAPPIST-1 e is 5° , and that of f is 1°) in the current simulation set. Obliquity can be larger depending on the initial

⁸ Changing $p\text{H}_2\text{O}$ at the model configuration stage only changes the surface pressure and the mean molecular weight; the actual water-vapor field is set entirely by moist processes such as evaporation, precipitation, and tracer transport through convection and circulation.

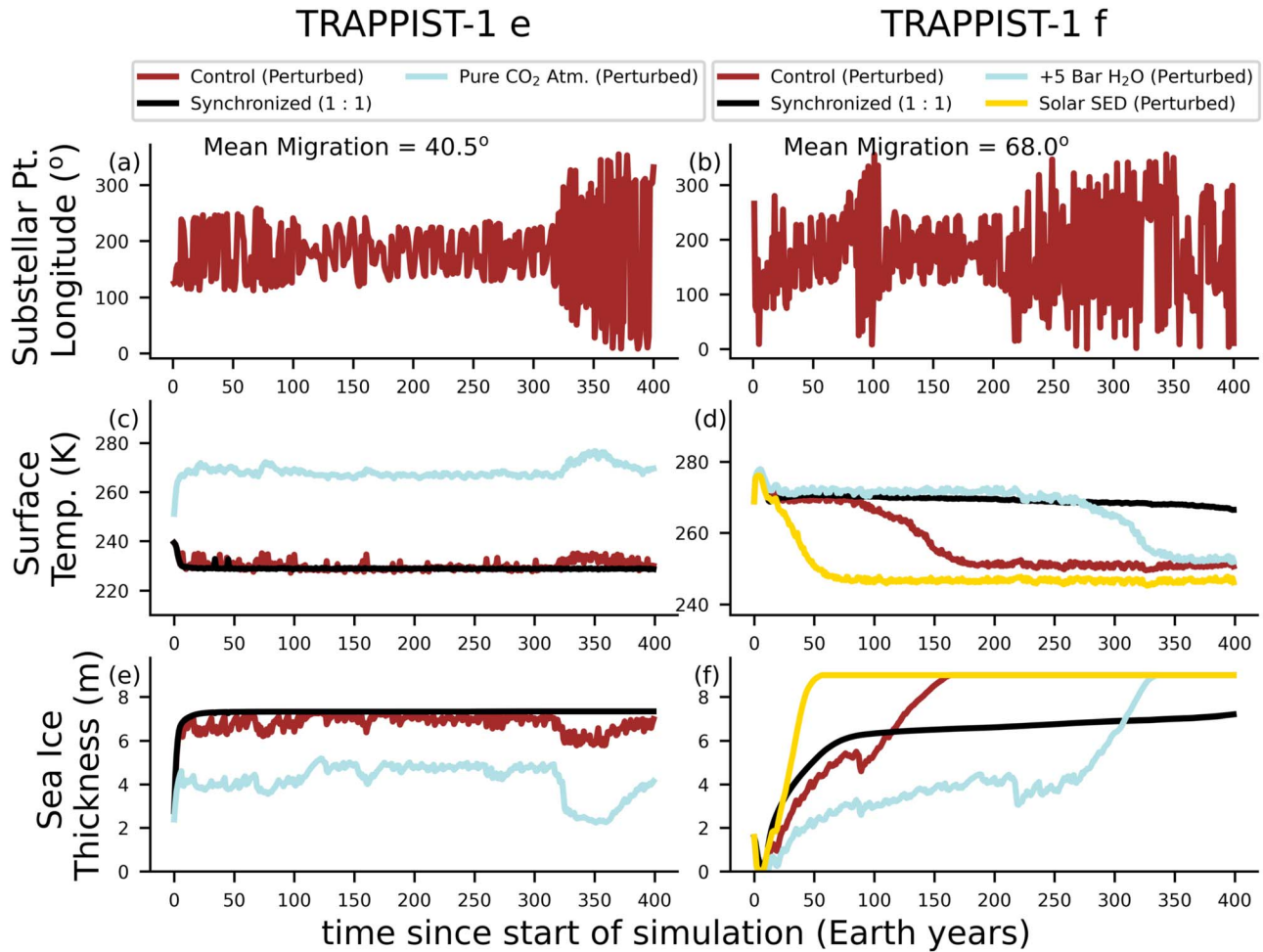


Figure 2. Time series of N-rigid-body simulation outcomes (a)–(b) that are used as inputs to the climate model results for TRAPPIST-1 e and f (c)–(f). The top panels show the substellar point longitude, and the bottom panels show global-mean surface temperatures and sea-ice thickness. The inclusion of sporadic planet interactions does not affect the mean climate of planet e, while increased pace of global glaciation is found for planet f with the inclusion of planet interactions. In the latter planet scenarios, as the location of maximum stellar heating moves away from the open ocean areas, the high surface albedo of the newly formed sea-ice makes deglaciation extremely difficult, and the planet rapidly transitions into a snowball state over ~ 200 yr. 180° is the substellar longitude for the 1 : 1 resonant state.

configurations, but we do not consider this in order to isolate the effects due to spin-axis misalignment.

One advantage of our modeling framework is the ability to consider the effects of spin dynamics on orbital evolution. In our numerical experiments of the TRAPPIST-1 planets as point-mass particles, this has shown to be relatively weak due to greater angular momentum of the orbit relative to planetary spin. However, this effect might be important for other planetary systems.

3. Results

Our results show that the libration of the substellar hemisphere due to mutual gravitational interactions between neighboring planets can substantially alter exoplanet climates at the outer edge of the habitable zone. We demonstrate this by comparing N-rigid-body simulation and climate model results of TRAPPIST-1 e and TRAPPIST-1 f. Synchronized planets (i.e., 1:1 resonance) will be hereafter referred to as unperturbed planets, whereas nonsynchronized planets (i.e., under the influence of planet interactions) will be referred to as perturbed planets.

For both TRAPPIST-1e and f, planet–planet interactions lead to nonstationary substellar longitudes. For planet e, the

migration remains small ($\sim 40^\circ$ longitude) until the system is sufficiently excited after year 330 (Figure 2(a)). On the contrary, for planet f, we find that the substellar point librates chaotically, deviates from that of the synchronized state and even at times passes through the antistellar position (near 360° longitude; Figure 2(b)). Only in certain time intervals (e.g., between 110 and 200 yr) does the substellar point linger around the original position. Comparing the substellar longitudinal evolution of planets e and f, in general the former has greater symmetry between the eastern and western hemispheres.

The most obvious feature of perturbed planets are the fluctuations in global-mean surface temperature and sea-ice thickness (Figures 2(c)–(f)), whereas the unperturbed planets have smoother temperature and sea-ice curves. For planet e, the T_s difference between the perturbed and unperturbed climates is small, even when substantial substellar point migration has been introduced at the later stages (Figure 2(c)). This can be seen by their partially overlapping temperature and sea-ice thickness curves. However, for planet f, the exact composition of the atmosphere or whether planet–planet interactions were present dramatically affected its evolutionary pathway. For instance, the T_s of the pure CO_2 atmosphere (control) becomes fully glaciated at year 175, whereas the $\text{CO}_2 + \text{H}_2\text{O}$ atmosphere enters that state at year 330 (Figure 2(d)). When

TRAPPIST-1 f

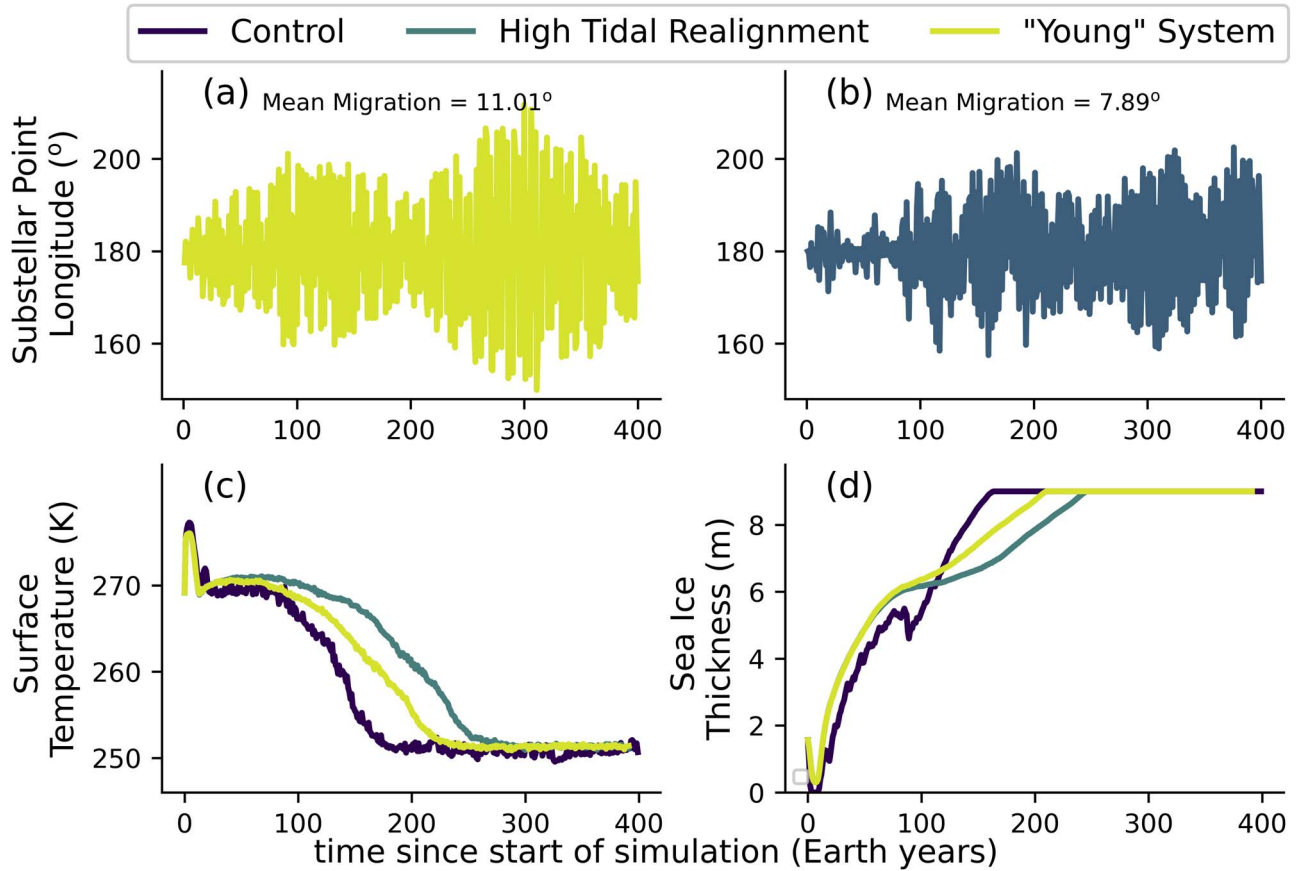


Figure 3. Time series of N-rigid-body simulation outcomes (a), (b) that are used as inputs to the climate model results for TRAPPIST-1 f (c), (d), exploring different levels of system excitation. The top panels show the substellar point longitude, and the bottom panels show global-mean surface temperatures and sea-ice thickness.

the rate of sea-ice formation of the perturbed control outpaces that of the unperturbed at year 100 (Figure 2(f)), the location of maximum stellar heating moves away from the open ocean areas, and the resultant high surface albedo of the newly formed sea-ice makes deglaciation extremely difficult.

However, a planetary system can exist in lower excited states than what has been discussed in Figure 2; whether these states would result in substantial sea-ice buildup deserves further investigation. Here, we find that for a younger system, the deviation of the substellar point from the 1:1 substellar longitude is only about 15° (Figure 3(a)). However, the degree of libration is most suppressed when the stellar tidal force from the host is elevated (Figure 3(b)). In this scenario, the first 80 yr have very synchronized orbits. Even after 100 yr, the average deviation is only 10° and never exceeding 20° throughout the full time series. We find that even with significant damping by tidal dissipation, the onset of runaway glaciation for the two less excited systems still occurs before the unperturbed (but after the control run), with fully ice-covered states reached at years 230 and 255 respectively⁹ between each simulation (Figures 3(c), (d)). This shows that the introduction of small amounts of stellar heating migration (10° – 20° longitude) away from the substellar cold-water region is enough to cause rapid sea-ice buildup. The much warmer planet e climates only

begin to glaciare when the system has been excited and the resultant libration becomes substantial, or $> 20^\circ$ (Figure 2(c)).

Figure 4 shows snapshots of surface temperatures averaged across various epochs for the control runs for each planet. Temperature maxima generally indicate the location of stellar heating, and when the shift in the location of substellar heating is rapid, remnant heat imprints can be preserved (Figure 4(a) and Figure 4(e)). On average, the T_s projections of planets e and f show much shallower day–night temperature gradients in comparison to those of the unperturbed planets (Figure 4(c) and Figure 4(d)). The 400 yr mean of planet e mirrors the transient/annual averages in terms of the relative location of stellar heating and T_s distribution (implying that climate equilibrium is quickly established with each change in the substellar longitude). For planet f, however, the temperature distributions at all three epochs are vastly different compared to those of the synchronized, reflecting the much greater influence of libration on climate in this regime. Overall, the most notable difference between planets e and f is the greater day–night and equator-to-pole temperature contrasts. The much thicker atmospheres needed to maintain open oceans for planet f (33 bar versus 1 bar of planet e) lead to more efficient heat transport and thus muted temperature contrasts.

Variabilities in surface air temperatures have major consequences for sea ice formation. Of the four scenarios shown, the only one devoid of any ice-free regions at year 400 is planet f control, which rapidly glaciates from the start, slowly

⁹ While these intervals seem short, the difference between the climate evolution tracks of each planet is likely much greater due to the high thermal inertia of more realistic ocean basins.

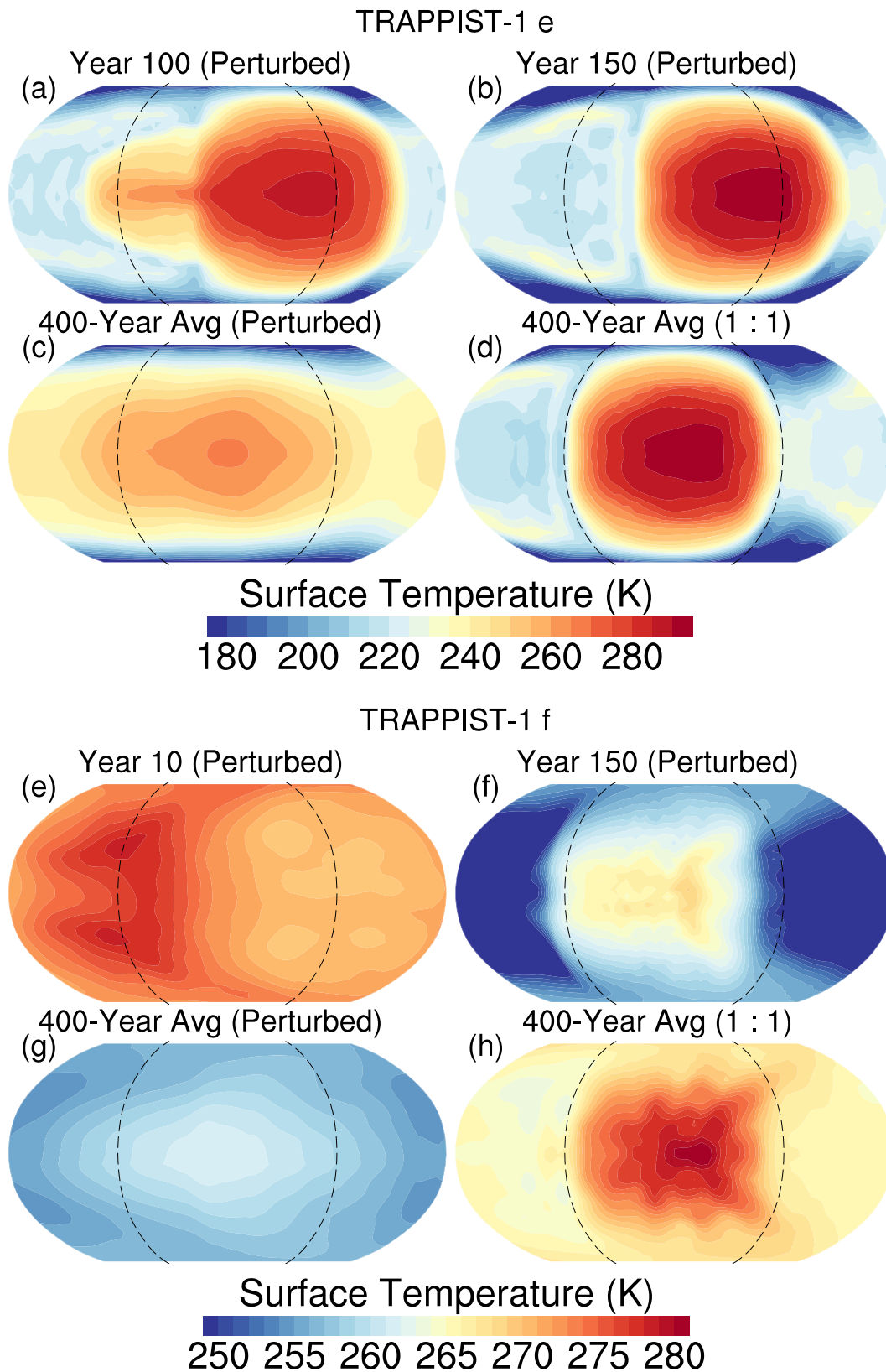


Figure 4. Map projections of sea surface temperature for perturbed planet e (year 100, year 150, and 400 yr averaged; (a), (b), and (c), respectively) and unperturbed planet e (d) as well as those for perturbed planet f (year 10, year 150, and 400 yr averaged; (e), (f), and (g), respectively) and unperturbed planet f (h). We find that time-averaged climates of perturbed scenarios deviate from a fixed 1:1 tidally locked unperturbed scenario, especially for planet f. The spatially and temporally varying temperature and albedos may imprint themselves in observations, e.g., thermal emission measurements, and potentially allow a measure of the planet's orbital and spin properties. The animated version shows the sea surface temperature evolution of planet f annually from 0 to 400 yr (left) and the time-averaged climate for the cumulative time period (right).

(An animation of this figure is available.)

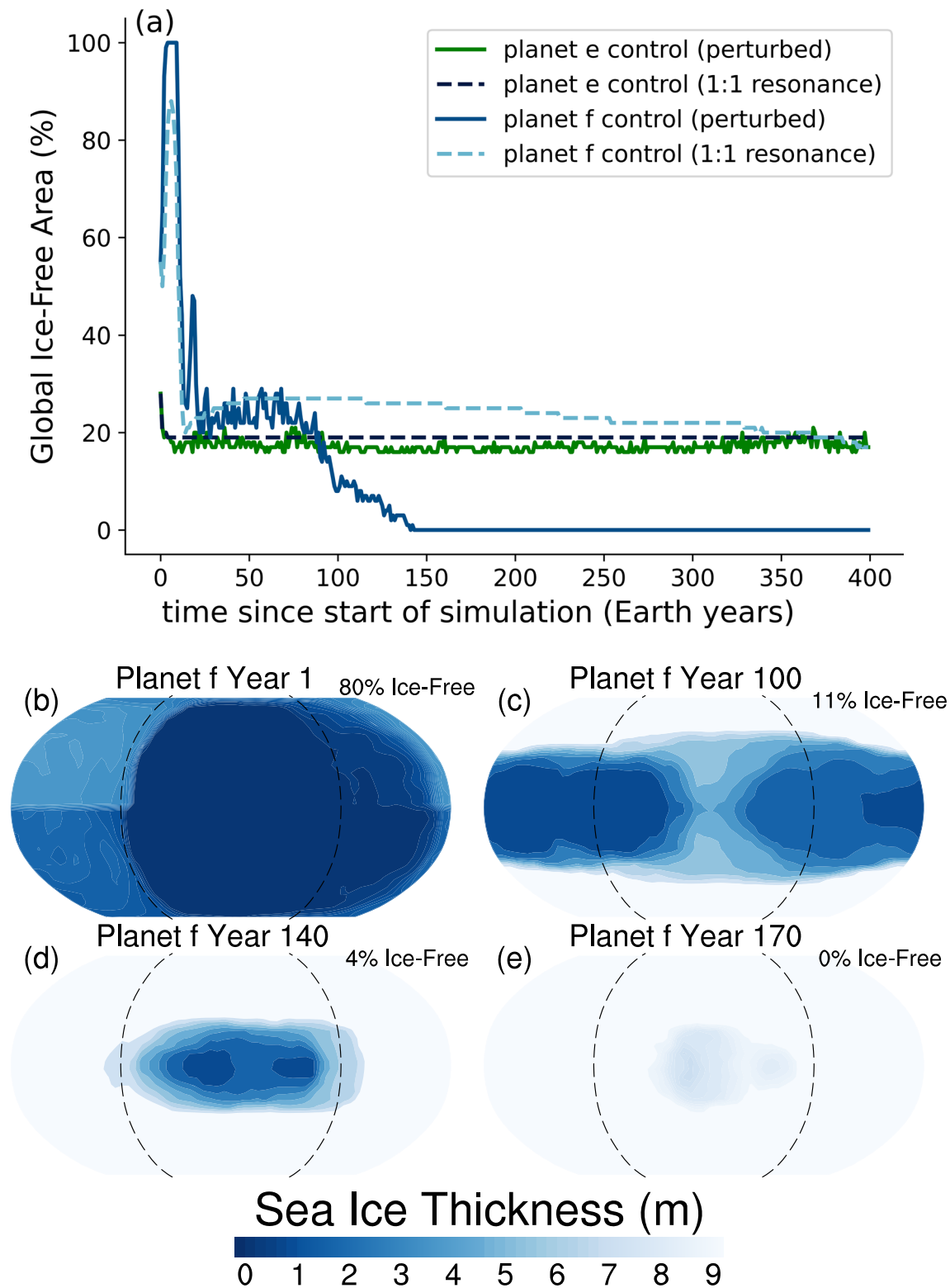


Figure 5. Temporal evolution of global ice-free fraction (a) and yearly averaged map projections of sea-ice thickness for planet f control at various epochs (b), (c), (d), and (e). Formation of sea ice is determined by the sea surface temperature. An animated adaptation of this figure is available. The animated version shows the yearly-mean sea-ice thickness evolution of planet f (left) and planet e (right).

(An animation of this figure is available.)

glaciates after ~ 30 yr, and then completely glaciates by the 140 yr mark (Figure 5(a)). The ice-free fraction of unperturbed planet f quickly decreases during the first 30 yr, slightly increases, and then returns to about 30% at year 300. Planet e experiences higher instellation and lower degrees of substellar

migration, leading to minimal differences in ice-free area fractions between the perturbed and unperturbed planets.

Figures 5(b)–(e) shows snapshots of sea-ice thickness for planet f control. As can be seen, the planet began with a full ocean cover (b), and as the the substellar point migrates away

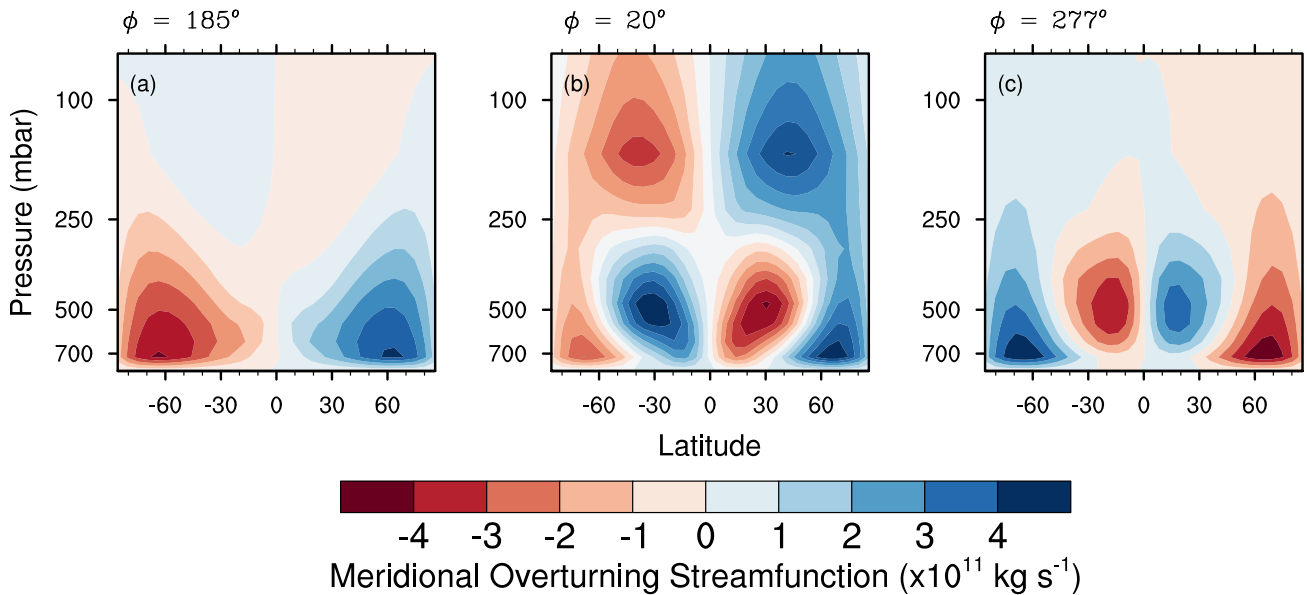


Figure 6. Hemispheric-mean mass streamfunctions at three snapshots in time for TRAPPIST-1 e with Earthlike atmospheres, averaged between longitudes 90° and 270° . We show that the patterns of the overturning circulation can be modified dramatically depending on the exact longitudinal location of stellar heating: (a) 185° , the original position, (b) 20° , near the antistellar point, and (c) 277° , at the terminator. The first scenario represents the 1:1 state, the second indicates downwelling at the ITCZ, and the third is an example of a “transitional” circulation pattern.

from the original location, the sea-ice closes in toward the equator, greatly elevating the surface albedo and making the planet more difficult to be heated due to the ice-albedo effect. At year 140, the remnant open ocean region is concentrated in the region of maximum stellar heating, leading to a familiar eyeball pattern. This pattern persists for 30–40 yr before eventually transitioning into a global snowball state (d). The differences in the above between planets e and f are largely due to the thicker atmospheres, lesser incident flux, and greater libration degrees of planet f. From the standpoint of the initial substellar hemisphere centered at 180° , it begins evolving from the warm state, and as the stellar flux is shifted longitudinally, the regime transitions into a glaciated state through rapid sea-ice buildup. When the substellar hemispheres librate back and the stellar flux here returns to the earlier value, the surface remains in a frozen state instead of the previous warm state it enjoyed and would require much greater stellar fluxes to deglaciate the planet. Conversely, none of the planet e cases display such a behavior as the higher stellar fluxes and thinner atmospheres remove the possibility of substantial climate bifurcation. With Earthlike atmospheric pressures, all planet e scenarios result in eyeball states (Figure 4(d)). Stronger instellation and reduced rate of substellar point migration allow these cases to sustain open oceans for much longer periods compared to those of planet f.

In addition to climate forcings, here we provide a glimpse of the effects of spin-orbit variations on atmospheric dynamics. As the planet librates longitudinally over ~ 100 yr, the zonally averaged flow across the entire globe is not substantially disrupted. However, between 90° and 270° longitudes, substantial shifts in the mass streamfunctions calculated from the Eulerian-mean meridional velocity and the generalized vertical coordinates can be seen (Figure 6). In the circulation regime of TRAPPIST-1 e when the substellar longitude is at 185° , eddy momentum and heat sources are minimal, and thus the differential diabatic heating is balanced only by adiabatic cooling (latent heating) near the substellar point and adiabatic

warming (radiative cooling) at higher latitudes, resulting in extended single cells in each hemisphere with strengths of $\sim 10^{11} \text{ kg s}^{-1}$. This situation does not hold when the substellar point shifts to 20° (Figure 6(b)). At this near-antistellar position (relative to the initial substellar hemisphere), the geometry of the meridional overturning circulation starts to reverse to a substellar-downwelling and high-latitude-upwelling pattern. At 277° , the mean flow transitions to mixtures between stronger tropical-to-midlatitude cells and weaker cells near the poles (Figure 6(c)). Overall, these results highlight unique circulation features on librating planets may have strong implications for day-to-nightside transport of dust, aerosols, and gas-phase species (see e.g., Carone et al. 2018; Boutle et al. 2020). Due to rapid homogenization of diabatic-heating-driven dynamics that mimic the mean flow of Earthlike rotators (Turbet et al. 2018), asynchronous worlds in higher SORs would not show such behavior in atmospheric dynamics and their variability.

4. Discussion

To date, the majority of climate modeling of rocky habitable zone (HZ) exoplanets has focused on synchronized planets and those with higher-order spin-orbit resonances (e.g., 3:2, 2:1, and 6:1), due to the assumed likelihood that most planets we have discovered will be in these states. Our results show that stochastic libration caused by secular gravitational interactions could modulate the climates of exoplanets in systems such as TRAPPIST-1.¹⁰

The orbital and spin trajectories of planets in compact systems have been investigated in several studies using

¹⁰ TRAPPIST-1 is found to be highly active in the X-ray and extreme UV, rendering its planets vulnerable to atmospheric erosion and making our atmospheric composition/pressure assumptions debatable ($\gtrsim 20$ bars; Roettenbacher & Kane 2017; Becker et al. 2020; Seli et al. 2021; Krissansen-Totton & Fortney 2022). However, the planetary parameters taken here were only used as a proof of concept to demonstrate climate variability in general, and our goal was not to make conclusions regarding the habitability of any particular world/system.

N-body/particle simulations (e.g., Rice et al. 2018; Vinson et al. 2019; Satyal et al. 2022). However, GRIT has a number of significant advantages over previous works. The majority of previous models (e.g., REBOUND, SymBA) assume that the planetary bodies or other objects are point-mass particles, and then spin-axis dynamics are calculated after the fact. Thus, the effects of planetary spin on their orbital dynamics are neglected. In addition, previous studies typically included a one-dimensional model to calculate spin evolution, and changes in obliquity (spin-orbit misalignment) were neglected (e.g., Vinson et al. 2019; Brasser et al. 2022). The inclusion of obliquity (effects in the z -direction) mediates and therefore reduces the degree of libration. GRIT, which is based on the first-principle rigid-body dynamics, provides more accurate results on the spin and orbital evolution. Future work will include a more detailed study on the statistical properties of spin variations based on different planetary tidal parameters and investigate the effects on climate and photochemistry.

Many authors have previously argued that planets at the outer edge of the habitable zone (OHZ) may be better candidates for biosignature and habitability-indicator targets as they are less susceptible to atmospheric escape and irreversible water loss (Lammer et al. 2011; Rogers et al. 2021) in comparison to those at the IHZ. Further, Colose et al. (2021) found that tidally heated planets with eccentric asynchronous orbits around cool stars may be able to maintain temperate climates even with stellar fluxes of $\sim 600 \text{ W m}^{-2}$ (Mars-like). However, the effects of tidal heating will likely be diminished for planets at the OHZ (Dobos et al. 2019), corresponding to those experiencing the largest degrees of libration in this work (i.e., change in 50° longitude in ~ 100 yr on average; Figure 1). In compact multiplanet systems, we argue that OHZ planets should rapidly transition into snowball states with modest-to-low stellar and tidal heating. When the stellar heating returns to its original position, the planet still remains in a snowball state. For temperate planets (those with fluxes between 900 and 1400 W m^{-2}), we agree with previous studies that they are the most promising targets for future atmospheric characterization campaigns. However, for single-planet systems or those without resonant chains, the spin-axis dynamical effects studied here do not come into play; hence, the conclusions cited above regarding the habitability of those planets are unchanged.

The most significant difference between our results and those using more complex GCMs (e.g., ExoCAM, ROCKE-3D, LMD, and UM) is the amount of greenhouse gas needed to substantially warm up surface air temperatures, especially in colder regimes of the HZ. Compared to Fauchez et al. (2019), our simulations require ~ 20 bars or more of CO_2 to substantially warm TRAPPIST-1 f (the results for TRAPPIST-1 e are the same). One likely explanation for this discrepancy is that ExoPlaSim and PlaSim heritage models place clouds at the substellar point of tidally locked models (Checlair et al. 2019; Paradise et al. 2019). Yet more advanced cloud models in state-of-the-art GCMs have shown that the daysides of tidally locked planets receiving lower stellar fluxes might be only partially cloudy. For example, the clear substellar skies found in GCM simulations typically have substellar point top-of-atmosphere (TOA) albedo of ~ 0.05 , whereas ExoPlaSim’s substellar point has a TOA albedo of 0.8 – 0.9 (since clouds are assumed to be gray). Different albedos would lead to differences in total energy budget and

therefore surface temperatures. Gaps in physical realism, for instance in modeling sea ice and convective processes, might also affect these predictions. Hence in certain regimes, e.g., the IHZ and OHZ where water cloud formation and condensation respectively become important, one would require verification or complementary experiments with more complex GCMs and with different radiative schemes. In any case, further model comparison efforts are needed to clarify these assumptions, parameterizations, and model uncertainties (e.g., Yang et al. 2019; Fauchez et al. 2021; Haqq-Misra et al. 2022).

In addition to climatic influences, those related to photochemistry and the formation of clouds and hazes may be markedly different if alternating regions of the planet are exposed to the star. For instance, the impact of stellar UV flare events (Paudel et al. 2021; Howard 2022; Louca et al. 2022) and stellar plasma (e.g., protons and α -particles; Tilley et al. 2019; Chen et al. 2021a) on varying sides of the hemisphere may lead to different global chemical and particle precipitation rates. Moreover, distinct atmospheric dynamics due to oscillating planetary spin (Figure 5) could drive the planet into other transport regimes (Carone et al. 2018; Chen et al. 2019) and change how chemical species and aerosols are advected from the dayside to the nightside (Boutle et al. 2020; Cohen et al. 2022). Modulations in the vertical mixing region and strength would lead to altered photolysis rates and shallower flux-abundance curves of biosignature gases.

Future work should also include the use of a fully coupled GCM with a dynamic ocean. Way & Georgakarakos (2017) studied the effects of variable eccentricity of Earthlike planets in the absence of Mars and found that relative humidity, precipitation, and sea-ice fraction vary on the order of ~ 5000 yr. Others have demonstrated how GCM simulations with the inclusion of ocean circulation and salinity can depart considerably from those established by slab ocean models. In addition to equilibrating on much longer timescales (500 – 1000 yr), coupled ocean models found increased regions of surface liquid water extending even to the nightsides due to the effects of ocean heat transport (Hu & Yang 2014; Del Genio et al. 2019; Olson et al. 2020; Salazar et al. 2020). At the OHZ, broadened open ocean basins would help delay the onset of the snowball states for planets under the influence of librating substellar hemispheres. Additionally, previous work ruled out the possibility of limit cycles on tidally locked M-dwarf planets due to the continuum of equilibrium states at all sea-ice fractions (Checlair et al. 2017, 2019). Our study suggests that hysteresis in this regime is still possible. However, the degree of hysteresis is likely small and may not necessarily entail the recovery of geochemical limit cycles driven by outgassing and carbon-silicate weathering. Further investigation with coupled ocean models is warranted to firmly establish the role of hysteresis in this regime.

Finally, the conclusions reached here are not strictly applicable to planets in tightly-packed M-dwarf systems experiencing mean motion resonances. A variety of strong planetary interactions can also lead to spin variations and dynamically interesting atmospheres. In the absence of these processes, one might assume that the planets in question would simply fall back to synchronized states.¹¹ However, the complete absence of external perturbers may be rare occurrences, as evidenced by the plethora of satellites in the solar

¹¹ Alternatively, if the planet has high eccentricity ($e > 0.2$), Renaud et al. (2021) showed that higher-order SOR configurations are the most plausible.

system and the high likelihood for the prevalence of (exo-) moons from recent surveys (Teachey & Kipping 2018). Further, many compact systems exist for multiple planets with K-star hosts, e.g., Kepler-411 and K2-266 (Rodriguez et al. 2018; Sun et al. 2019), suggesting that our implications for the OHZ are relevant for planetary systems beyond those that are TRAPPIST-1-like, and even extend to planets born with a variety of rotation rates around Sunlike stars (Kane 2019; Guzewich et al. 2020). Binary systems may also be sites for such perturbations, but the stability of their planetary orbits is debatable (see, e.g., Forgan 2016; Quarles et al. 2022). These possibilities will need to be examined with different star-planet-disk boundary conditions such as initial dynamical frictions in order to assess the competition between the strength of host-star tidal realignment and external interactions with other rocky bodies.

5. Conclusion

Exoplanets residing in multiplanet compact systems are often assumed to be lodged in 1:1, 3:2, and 2:1 resonant chains. However, sporadic and highly variable planetary spins and orbits may have drastic climate and atmospheric consequences. Here, for the first time, an N-rigid-body spin-orbital integrator is used in conjunction with a GCM to investigate the climate of TRAPPIST-1 e and f under the influence of host-star tides and planet-planet interactions. We find that the secular gravitational interactions between mutual orbits in compact systems can drive planets out of synchronized states, affecting their evolving and mean climates. This effect is particularly dramatic for planets further away from the host star, due to reduced strength of tidal dissipation. We further find that it is challenging to sufficiently warm planets at the outer edge of the habitable zone (even with CO₂-rich atmospheres in excess of 30 bars) due to greater degrees of substellar longitude migration and increased climate hysteresis. As this drift occurs on decadal timescales, it allows the formation of new sea-ice, which increases the surface albedo of the planet, making subsequent deglaciation by stellar heating difficult. Our study suggests that OHZ planets in compact systems are less likely to have significant regions of open ocean basins, even with >1–10 bars of greenhouse-gas warming.


Temporally and spatially variable temperature contrasts between the day and nightsides of these planets could manifest themselves in secondary eclipse thermal emission spectra, potentially offering clues to the planets' spin-orbit states. Moving forward, we will employ climate models in conjunction with N-body or N-rigid-body simulations to systematically investigate the effects of planetary orbit and spin characteristics on exoplanet climate and atmospheric observables.

Goddard affiliates acknowledge support from the GSFC Sellers Exoplanet Environments Collaboration (SEEC), which is supported by NASA's Planetary Science Division's Research Program. H.C. is supported by an appointment to the NASA Postdoctoral Program at Goddard Space Flight Center, administered by Oak Ridge Associated Universities under contract with NASA. G.L. is grateful for the support by NASA 80NSSC20K0641 and 80NSSC20K0522. We acknowledge high-performance computing support from Cheyenne (<https://doi.org/10.5065/D6RX99HX>) provided by NCAR's Computational and Information Systems Laboratory, sponsored by the National Science Foundation. This work used the Hive cluster,

which is supported by the National Science Foundation under grant number 1828187.

Software: GRIT (Chen et al. 2021b), ExoPlaSim (Paradise et al. 2022). The Python scripts for the climate model, input data, and codes to post-process and visualize the results is available on GitHub: https://github.com/hwchen1996/sporadic_climate.

ORCID iDs

Howard Chen  <https://orcid.org/0000-0003-1995-1351>
 Gongjie Li  <https://orcid.org/0000-0001-8308-0808>
 Adiv Paradise  <https://orcid.org/0000-0001-6774-7430>
 Ravi K. Kopparapu  <https://orcid.org/0000-0002-5893-2471>

References

- Agol, E., Dorn, C., Grimm, S. L., et al. 2021, *PSJ*, 2, 1
 Barnett, M. N., & Olson, S. L. 2022, *PSJ*, 3, 132
 Becker, J., Gallo, E., Hodges-Kluck, E., Adams, F. C., & Barnes, R. 2020, *AJ*, 159, 275
 Benneke, B., Wong, I., Piaulet, C., et al. 2019, *ApJL*, 887, L14
 Biasiotti, L., Simonetti, P., Vladilo, G., et al. 2022, *MNRAS*, 514, 5105
 Bolmont, E., Demory, B. O., Blanco-Cuaresma, S., et al. 2020, *A&A*, 635, A117
 Boutle, I. A., Joshi, M., Lambert, F. H., et al. 2020, *NatCo*, 11, 2731
 Braam, M., Palmer, P. I., Decin, L., et al. 2022, *MNRAS*, 517, 2383
 Brasser, R., Pichierri, G., Dobos, V., & Barr, A. C. 2022, *MNRAS*, 515, 2373
 Carone, L., Keppens, R., Decin, L., & Henning, T. 2018, *MNRAS*, 473, 4672
 Checlair, J., Menou, K., & Abbot, D. S. 2017, *ApJ*, 845, 132
 Checlair, J. H., Olson, S. L., Jansen, M. F., & Abbot, D. S. 2019, *ApJL*, 884, L46
 Chen, H., & Jacobson, S. A. 2022, *E&PSL*, 594, 117741
 Chen, H., Wolf, E. T., Zhan, Z., & Horton, D. E. 2019, *ApJ*, 886, 16
 Chen, H., Zhan, Z., Youngblood, A., et al. 2021a, *NatAs*, 5, 298
 Chen, R., Li, G., & Tao, M. 2021b, *ApJ*, 919, 50
 Cohen, M., Bolasina, M. A., Palmer, P. I., et al. 2022, *ApJ*, 930, 152
 Colose, C. M., Del Genio, A. D., & Way, M. J. 2019, *ApJ*, 884, 138
 Colose, C. M., Haqq-Misra, J., Wolf, E. T., et al. 2021, *ApJ*, 921, 25
 Cooke, G. J., Marsh, D. R., Walsh, C., Rugheimer, S., & Villanueva, G. L. 2023, *MNRAS*, 518, 206
 Deitrick, R., Barnes, R., Bitz, C., et al. 2018a, *AJ*, 155, 266
 Deitrick, R., Barnes, R., Quinn, T. R., et al. 2018b, *AJ*, 155, 60
 Del Genio, A. D., Way, M. J., Amundsen, D. S., et al. 2019, *AsBio*, 19, 99
 Dobos, V., Barr, A. C., & Kiss, L. L. 2019, *A&A*, 624, A2
 Edwards, B., Changeat, Q., Mori, M., et al. 2021, *AJ*, 161, 44
 Eggleton, P., Kiseleva, L. G., & Hut, P. 1998, *ApJ*, 499, 2
 Fauchez, T. J., Turbet, M., Sergeev, D. E., et al. 2021, *PSJ*, 2, 106
 Fauchez, T. J., Turbet, M., Villanueva, G. L., et al. 2019, *ApJ*, 887, 194
 Forgan, D. 2016, *MNRAS*, 463, 2768
 Fraedrich, K., Jansen, H., Kirk, E., Luksch, U., & Lunkeit, F. 2005, *MetZe*, 14, 299
 Fu, G., Espinoza, N., Sing, D. K., et al. 2022, *ApJ*, 940, L35
 Galuzzo, D., Cagnazzo, C., Berrilli, F., Fierli, F., & Giovannelli, L. 2021, *ApJ*, 909, 191
 Guzewich, S. D., Lustig-Yaeger, J., Davis, C. E., et al. 2020, *ApJ*, 893, 140
 Hammond, M., & Lewis, N. T. 2021, *PNAS*, 118, e2022705118
 Haqq-Misra, J., Wolf, E. T., Fauchez, T. J., Shields, A. L., & Kopparapu, R. K. 2022, *PSJ*, 3, 260
 He, F., Merrelli, A., L'Ecuyer, T. S., & Turnbull, M. C. 2022, *ApJ*, 933, 62
 Howard, W. S. 2022, *MNRAS*, 512, L60
 Hu, Y., & Yang, J. 2014, *PNAS*, 111, 629
 Jansen, T., Scharf, C., Way, M., & Del Genio, A. 2019, *ApJ*, 875, 79
 Jernigan, J., Laffèche, É., Burke, A., & Olson, S. 2023, *ApJ*, 944, 205
 Joshi, M. M., Elvidge, A. D., Wordsworth, R., & Sergeev, D. 2020, *ApJL*, 892, L33
 Kaltenecker, L., & Lin, Z. 2021, *ApJL*, 909, L2
 Kane, S. R. 2019, *AJ*, 158, 72
 Kane, S. R. 2021, Planetary Habitability (Bristol: IOP Publishing)
 Kane, S. R., Hinkel, N. R., & Raymond, S. N. 2013, *AJ*, 146, 122
 Kawamura, K., Parrenin, F., Lisiecki, L., et al. 2007, *Natur*, 448, 912
 Kilic, C., Raible, C. C., & Stocker, T. F. 2017, *ApJ*, 844, 147
 Kopparapu, R. K., Wolf, E. T., Arney, G., et al. 2017, *ApJ*, 845, 5

- Kreidberg, L., Bean, J. L., Désert, J.-M., et al. 2014, *Natur*, **505**, 69
- Krissansen-Totton, J., & Fortney, J. J. 2022, *ApJ*, **933**, 115
- Lammer, H., Eybl, V., Kisllyakova, K. G., et al. 2011, *Ap&SS*, **335**, 39
- Laskar, J., Robutel, P., Joutel, F., et al. 2004, *A&A*, **428**, 261
- Lean, J., Beer, J., & Bradley, R. 1995, *GeoRL*, **22**, 3195
- Leconte, J., Wu, H., Menou, K., & Murray, N. 2015, *Sci*, **347**, 632
- Lefèvre, M., Turbet, M., & Pierrehumbert, R. 2021, *ApJ*, **913**, 101
- Lingam, M., Pryor, S., & Ginsburg, I. 2022, *MNRAS*, **510**, 4837
- Louca, A. J., Miguel, Y., Tsai, S.-M., et al. 2022, arXiv:2204.10835
- Lustig-Yaeger, J., Meadows, V. S., & Lincowski, A. P. 2019, *AJ*, **158**, 27
- Lustig-Yaeger, J., Sotzen, K. S., Stevenson, K. B., et al. 2022, *AJ*, **163**, 140
- Méndez, A., Rivera-Valentín, E. G., Schulze-Makuch, D., et al. 2021, *AsBio*, **21**, 1017
- Mikal-Evans, T. 2022, *MNRAS*, **510**, 980
- Olson, S. L., Jansen, M., & Abbot, D. S. 2020, *ApJ*, **895**, 19
- Paradise, A., Macdonald, E., Menou, K., Lee, C., & Fan, B. L. 2022, *MNRAS*, **511**, 3272
- Paradise, A., Menou, K., Valencia, D., & Lee, C. 2019, *JGRE*, **124**, 2087
- Paudel, R. R., Barclay, T., Schlieder, J. E., et al. 2021, *ApJ*, **922**, 31
- Poulsen, C. J., Pierrehumbert, R. T., & Jacob, R. L. 2001, *GeoRL*, **28**, 1575
- Quarles, B., Li, G., & Lissauer, J. J. 2022, *MNRAS*, **509**, 2736
- Renaud, J. P., Henning, W. G., Saxena, P., et al. 2021, *PSJ*, **2**, 4
- Rice, D. R., Rasio, F. A., & Steffen, J. H. 2018, *MNRAS*, **481**, 2205
- Rodriguez, J. E., Becker, J. C., Eastman, J. D., et al. 2018, *AJ*, **156**, 245
- Roettenbacher, R. M., & Kane, S. R. 2017, *ApJ*, **851**, 77
- Rogers, J. G., Gupta, A., Owen, J. E., & Schlichting, H. E. 2021, *MNRAS*, **508**, 5886
- Salazar, A. M., Olson, S. L., Komacek, T. D., Stephens, H., & Abbot, D. S. 2020, *ApJL*, **896**, L16
- Satyal, S., Quarles, B., & Rosario-Franco, M. 2022, *MNRAS*, **516**, 39
- Seli, B., Vida, K., Moór, A., Pál, A., & Oláh, K. 2021, *A&A*, **650**, A138.
- Sergeev, D. E., Lewis, N. T., Lambert, F. H., et al. 2022, *PSJ*, **3**, 214
- Shields, A. L., Barnes, R., Agol, E., et al. 2016, *AsBio*, **16**, 443
- Spiegel, D. S., Raymond, S. N., Dressing, C. D., Scharf, C. A., & Mitchell, J. L. 2010, *ApJ*, **721**, 1308
- Sun, L., Ioannidis, P., Gu, S., et al. 2019, *A&A*, **624**, A15
- Swain, M. R., Estrela, R., Roudier, G. M., et al. 2021, *AJ*, **161**, 213
- Tamayo, D., Cranmer, M., Hadden, S., et al. 2020, *PNAS*, **117**, 18194
- Teachey, A., & Kipping, D. M. 2018, *SciA*, **4**, eaav1784
- Tilley, M. A., Segura, A., Meadows, V. S., Hawley, S., & Davenport, J. 2019, *AsBio*, **19**, 64
- Toon, O. B., Pollack, J. B., Ward, W., Burns, J. A., & Bilski, K. 1980, *Icar*, **44**, 552
- Touma, J., & Wisdom, J. 1994, *AJ*, **107**, 1189
- Turbet, M., Bolmont, E., Leconte, J., et al. 2018, *A&A*, **612**, A86
- Vallis, G. K., Colyer, G., Geen, R., et al. 2018, *GMD*, **11**, 843
- Vervoort, P., Horner, J., Kane, S. R., Turner, S. K., & Gilmore, J. 2022, *AJ*, **164**, 130
- Vinson, A. M., Tamayo, D., & Hansen, B. M. S. 2019, *MNRAS*, **488**, 5739
- Way, M. J., Del Genio, A. D., Kiang, N. Y., et al. 2016, *GeoRL*, **43**, 8376
- Way, M. J., & Georgakarakos, N. 2017, *ApJL*, **835**, L1
- Wolf, E. T., Kopparapu, R., Haqq-Misra, J., & Faucher, T. J. 2022, *PSJ*, **3**, 7
- Wordsworth, R., & Kreidberg, L. 2022, *ARA&A*, **60**, 159
- Wunderlich, F., Scheucher, M., Godolt, M., et al. 2020, *ApJ*, **901**, 126
- Yang, J., Abbot, D. S., Koll, D. D. B., Hu, Y., & Showman, A. P. 2019, *ApJ*, **871**, 29
- Yang, J., Boué, G., Fabrycky, D. C., & Abbot, D. S. 2014, *ApJL*, **787**, L2
- Yang, J., Cowan, N. B., & Abbot, D. S. 2013, *ApJL*, **771**, L45